Crystal rotation and microstructures in an aluminum single-slip system under tensile loading

Yutaka Yoshida[1]*, Jun-ichi Shibano[1], Ken-ichi Fukuda[2, 6], Kengo Terabayashi[2, 7], Masato Eguchi[2, 8], Kentaro Kajiwara[3], Takahisa Shobu[4], and Ayumi Shiro[5]

[1] *Faculty of Engineering, Kitami Institute of Technology, Koen-cho, Kitami, Hokkaido 090-8507, Japan*

[2] *Graduate Students, Department of Mechanical Engineering, Kitami Institute of Technology, Koen-cho, Kitami, Hokkaido 090-8507, Japan*

[3] *Japan Synchrotron Radiation Research Institute (JASRI), Kouto, Sayo-cho, Sayo-gun, Hyogo 679-5198, Japan*

[4] *Quantum Beam Science Center, Japan Atomic Energy Agency (JAEA), Kouto, Sayo-cho, Sayo-gun, Hyogo 679-5148, Japan*

[5] *National Institutes for Quantum and Radiological Science and Technology (QST), Kouto, Sayo-cho, Sayo-gun, Hyogo 679-5148, Japan*

[6] Present address: *Yamazaki Mazak Corporation, Takeda, Oguchi, Niwa, Aichi, 480-097, Japan*

[7] Present address: *YKKAP Inc., Sugimoto, Namerikawa, Toyama, 936-8510, Japan*

[8] Present address: *MinebeaMitsumi Inc., asana, Hukuroi, Shizuoka, 437-1102, Japan*

***E-mail:** **yyoshida@mail.kitami-it.ac.jp**

Abstract

We experimentally investigated the rotation angle of the (220) plane in an aluminum single-slip system in which the angles of <110> and <111> in the single crystal were 45° relative to the tensile loading direction. Crystal rotation was investigated at several spots (50 × 50 μm) along <110> and <111> using synchrotron radiation white X-rays at the BL28B2 beamline of super photon ring-8. In measurements along the <110> axis, at an applied strain of ε = 5%, the relative crystal rotation of (220) in the vertical plane increased from 0.850° to 5.438° in the range of 0.9 to 1.4 mm. We observed the microstructure using a transmission electron microscope and verified the size of the dislocation cells or subgrains at each spot along <110>. The fundamental local crystallography revealed in this work should be helpful in establishing a method for evaluating ductile damage in materials.

Keywords: Aluminum single crystal; Crystal rotation; Nonuniform strain; Synchrotron white X-ray; Profile fitting

1. Introduction

In recent years, crystal plasticity modeling has been studied for application to cold rolling [1, 2]. The microstructure and local crystallography of the face-centered-cubic (FCC) single crystals of aluminum (Al) have been studied to understand crystal plasticity, and their various slip systems have been evaluated through calculations. Fundamental studies on controlling the fracture of an Al single crystal have also been reported [3–9]. Analytical methods based on X-ray diffraction (XRD) profiles have been used to characterize the ductile damage of Al under plastic deformation because the X-ray measurements of Al single crystals are known to reflect the damage sustained by the material [10–12]. When evaluating ductile damage, analyses of the integrated intensity and the full-width at half-maximum (FWHM) of the peaks in the XRD pattern are important because the attributes of the peaks change with the origin of the nonuniform strain and the crystalline size [13–17].

Studies of stress and strain in materials using synchrotron radiation (SR) have recently been reported [18, 19]. We previously performed measurements of diffracted X-rays with Al single crystals using SR white X-rays at the super photon ring-8 facility and reported on the ductile damage in a notched Al single crystal under tensile load at room temperature. Our results clarified the distribution of nonuniform strain during ductile damage progression in the four-slip system [20]. Based on these results, we estimated the generation behavior and orientation of subgrains and their correlation with the crystal orientation. The results show that subgrains were generated and rotated near the notch and that the angle variations in the vertical plane were large compared with those in the horizontal plane. Furthermore, the influence of ductile damage progression on the strain energy was expected because the dislocation density increased; however, it was relatively low near the notch. Nonuniform strain was also demonstrated to increase along the 45° direction near the notch [21]. However, in previous research, the distribution along the direction of 45° in the Al single crystal of a single-slip system was unclear when single-notch specimens were used.

In this study, we measured the diffraction X-ray of the (220) plane in an Al single crystal of a single-slip system using a double-notched specimen. Measurements were conducted under applied strains of ε = 1% and ε = 5%; the measurements were conducted using white X-rays at the SR facility at the BL28B2 beamline of SPring-8, which has a spot size of 50 × 50 μm (height × width). The distribution of the crystal rotation of the <110> axis from the notch of the specimen was verified under tensile loading via white XRD. Furthermore, from the tensile specimen after the SR white X-ray measurements, a sample for transmission electron microscopy (TEM) was prepared, and the microstructures were observed. The size of the dislocation cell or subgrain and the dislocation density were verified at the local area along <110> from the notch. We discuss the distribution of the crystal rotation of the <110> axis and miniaturization at the local area along <110> in an Al single crystal of a single-slip system under tensile loading.

2. Experimental Procedure

2.1 Specimen

Al single crystals of 6N purity (99.9999% pure) with <111> and <110> crystal orientations, which have a 45° slant relative to the tensile loading direction, were prepared from a crystalline disk by using a low-speed diamond cutter. The tensile loading test specimen of an Al single crystal was prepared in I-type geometry with a double notch by using wire electric discharge machining [20]. As shown in Fig. S1, the double notch was 0.4-mm wide and 0.3-mm deep on both sides of the center of the parallel part. Figure S2 shows the corresponding stress-strain curve during the tensile test.

2.2 *Measurement facility and conditions*

The tensile loading test during the measurement of the transmitted diffraction X-rays was performed using compact tension equipment installed in the SR facility at SPring-8 (Fig. S3). Laue patterns were confirmed

using a flat-panel sensor for each condition [8, 9, 20, 21]. The semiconductor detector was oriented at a horizontal diffraction angle of 6° to the incident white X-rays.

The slits installed at both the irradiation and the detector sides were 50 μm high and 50 μm wide. Fig. S4 shows the gauge volume of this measurement under tensile loading. Therefore, the energy-dispersive XRD technique was used to irradiate the specimen at a Bragg angle θ of 3° to the white X-ray beam. The measurement of the detected diffracted X-rays during the tensile testing was discriminated into 4096 channels by a multichannel analyzer (MCA). The measured energy width per channel was 58.8 eV, and energies as high as approximately 241 keV could be discriminated into 4096 channels. Radioactive isotopes of Co-57 and Am-241 were used to calibrate the energy according to the following equation (Figure S5):

$$E_n = 0.0588 \times CH + 0.3081 \ [keV] \qquad (1)$$

,

where *CH* is the channel number of the MCA.

The measurement spots were in a region located 0.05 mm in the horizontal and vertical directions from the tip of the notch as the base point S, and the measurements were measured at the spots at intervals of 0.1 mm with <110> and <111> each inclined 45° with respect to the tensile direction in the single-slip system. Before tensile loading, we measured the five points near the center of the specimen for 90 s per point under the no-loading condition. The average value of the peak energy of each lattice plane was converted into nonstrain data. Each spot from the notch was measured under the applied strains of $\boldsymbol{\varepsilon}$ = 1% and $\boldsymbol{\varepsilon}$ = 5%. The measurement spots are shown in Fig. 1. The measurements were performed for 60 s per spot. During the measurements, the loading was stopped, and the distance between grips was maintained. The angle of the rotated specimen was measured at each spot by using the flat-panel sensor installed in the detector side. The diffraction X-rays that penetrated the specimen were detected, as shown in Fig. S6. After detection, we

adjusted the relative rotation angle of the specimen for each spot after the specimen transmitted the diffracted X-rays. Furthermore, we arranged the spot symmetrically with respect to a center on the flat-panel sensor, and the relative rotation angle was determined via adjustment to maximize the diffraction X-ray intensity.

2.3 Profile fitting

To investigate the ductility damage progress, profile fitting of the peak in the measured diffraction X-ray profile was performed using the Gauss function expressed by Eq. (2):

$$I = I_0 + \frac{A}{w\sqrt{\frac{\pi}{2}}} e^{-2\frac{(x-x_c)^2}{w^2}} \qquad (2)$$

,

where I_0 is the background intensity, A is the integrated intensity of a diffraction profile, x is the diffraction angle 2θ, x_c is a peak diffraction angle $2\theta_c$, and w is twice the standard deviation.

2.4 ***TEM sample preparation***

For TEM observations, an Al single crystal after tensile loading was cut to dimensions of 2.6 × 1.0 × 2.0 mm using a diamond cutter. Subsequently, the thickness of the specimen was carefully polished to 0.1 mm. The hole for TEM observation was formed at positions approximately 0.7 and 1.2 mm from the notch using an ion slicer (JEOL EM-09100IS). The Ar^+-ion beam conditions were an irradiation angle of 1.8° and an accelerating voltage of 3.0 to 6.0 kV. TEM samples were prepared for observing the dislocations in the areas 0.6 and 0.8 mm from the notch (Fig. S7) and 1.1 and 1.3 mm from the notch (Fig. S8). Microstructure

observations after tensile loading were performed on a Hitachi H-9000NR transmission electron microscope. The size of the dislocation cells or subgrains was determined from their microstructures.

3. Results and Discussion

3-1. Crystal rotation under tensile loading

Figure 2 shows the relative rotation angles of the normal direction of the (220) diffraction plane in the horizontal and vertical planes. As shown in Fig. 2(a), the angle in the horizontal plane indicates that neither the <110> nor the <111> direction rotates. However, in the vertical plane as shown in Fig. 2(b), the trend of the <110> measurements at $\boldsymbol{\varepsilon}$ = 1% was identical to that observed in the range between the notch and 1.5 mm; for ε = 5%, the angle (blue) then increased from 0.850° to 5.438° in the range of 0.9–1.4 mm. Hence, the result of <110> is a crystal rotation similar to that of the cold-rolled Al single crystals [1]. In the measurements (brown) along <111>, the trend increased from 1.895° to 4.538° in the range of 1.1–1.4 mm. These results are attributed to the activity of the dislocations induced by the slip on the Al (111) plane, thus suggesting that the distribution of the relative rotation angle correlates with the generated dislocation cell size and density in the microstructure.

3-2. Distributions of integrated intensity and full-width at half-maximum

To compare the amount of subgrains and nonuniform strain, we determined the integrated intensity and FWHM using Gaussian functions. The distribution of integrated intensity determined from the XRD profile is shown in Fig. 3(a). At an applied strain $\boldsymbol{\varepsilon}$ = 1%, the integrated intensity in measurements of <110> and <111> was low (green and yellow) from 0 to 0.4 mm. The integrated intensity of <110> became high in the range of 0.7–1.5 mm in both directions. This result indicates that fine-grained structures were present, which is consistent with the XRD results. In general, subgrains are generated in a single crystal as ductile

damage progresses [4, 7, 21]. Subgrains that accompany the development of a slip band due to ductile damage develop near the notch. In the measurement of <111>, at $\boldsymbol{\varepsilon}$ = 5%, although the integrated intensity is low from 0 to 0.3 mm, it becomes relatively high after 0.4 mm. The value of the <110> is low near the notch, and the peak intensity increases at the spot that is 0.7 mm from the notch. At an applied strain of $\boldsymbol{\varepsilon}$ = 5%, the integrated intensity decreases in both directions. In particular, the measurements of <110> show that the integrated intensity decreases near the notch (from 0 to 0.3 mm) and at the intersection of <110> and <111> (from 1.2 to 1.4 mm).

Fig. 3(b) shows the distribution of the FWHM values determined from the XRD profiles. For $\boldsymbol{\varepsilon}$ = 1%, the FWHM (green) of <110> increases from 0.47 to 0.55 in the range of 0–0.7 mm, and a large FWHM (green: 0.52414 to 0.53133) is observed from 0.8 to 1.5 mm. On the other hands, the FWHM (yellow) of <111> increase from 0.47 to 0.55 in the range between 0 and 0.7 mm, and decreases from 0.55078 to 0.50363 in the range between 0.7 and 0.9 mm; then, the FWHM<111> of becomes nearly constant (about 0.51). The distribution of the FWHM values suggests that the nonuniform strain was high in the range from 0.8 to 1.3 mm along <110>. For ε = 5%, the FWHM values decreased. In particular, the value of <110> decreased from 0.50585 to 0.48524 in the range between 0.9 and 1.4 mm. The decrease in nonuniform strain is attributed to the release of strain energy.

3-3. Microstructures in Al single crystals

To characterize the localized crystal rotation after a strain of ε = 5% was applied, we observed microstructures at 0.6, 0.8, 1.1, and 1.3 mm from the notch along <110>. Figure 4 shows the TEM images of each area. At the 0.6 mm area, dislocations were observed along <110> and <111>; furthermore, the entanglements of dislocations were confirmed along <110> and along the tensile direction in Fig. 4(a). At 0.8 mm, dislocation cells were observed in Fig. 4(b). At 1.1 and 1.3 mm, subgrains were observed, and dislocation cells of approximately 100 nm or smaller were also observed in each spot, as shown in Figs. 4(c) and 4(d).

Figure 5 shows the enlarged TEM images of each area. In the area 0.6 mm from the notch, the entanglement of dislocations occurred only in the local area. The size of the dislocation cells confirmed in the local area is approximately 100 nm on average (Fig. 5(a)). The dislocation density calculated from Ham's formula [22] was 0.65×10^{14} m^{-2}. In the area 0.8 mm from the notch, a uniform distribution of dislocations was observed. The size and the dislocation density were determined to be 275 nm and 0.83×10^{14} m^{-2} on average, respectively (Fig. 5(b)). In the areas 1.1 and 1.3 mm from the notch, the size of the dislocation cells decreased. The size and the dislocation density were determined to be 150 nm and 1.00×10^{14} m^{-2} on average, respectively (Fig. 5(c)). The entanglement of dislocations was observed, and their size decreased to approximately 50 nm. The dislocation density was 0.91×10^{14} m^{-2} on average (Fig. 5(d)). The reduction of dislocation density is attributed to the release of strain energy at the intersection of the plastic strains occurring in the direction along 45° from the notch. These results correlate with the plastic strain generated in the direction along 45° from the notch; the increased crystal rotation at the intersection, as determined from the XRD results, also implying that in the single-slip system, the damage during ductile fracture is generated at the intersection. As the damage progresses, the dislocation density decreases owing to the activity of dislocations. Considering that the development of a slip band leads to a release of local strain energy and nonuniform strain, it is considered that the crystal rotation increases locally.

4. Conclusions

Using a double-notched specimen and SR white X-ray, we performed a correlation analysis between the crystal rotation angle and a spot from the notch in the direction of 45° to <111> and <110> under tensile loading. Furthermore, we used TEM to examine the crystal rotation and microstructure in the specimens to characterize their microstructures after the tensile loading tests. Our main conclusions are summarized as follows:

(1) The crystal rotation angle with the progression of ductile damage was larger in the vertical plane than that in the horizontal plane. In the measurement along <110>, the relative rotation angle was the maximum at the intersection of <111> and <110>.

(2) The integrated intensity and the FWHM decreased near the notch (from 0 to 0.3 mm) as well as at the intersection of <110> and <111> in the measurement along <110>.

(3) The dislocation cell size and the dislocation density decreased at the intersection of <111> and <110> in the measurement of <110> for $\boldsymbol{\varepsilon}$ = 5%. This behavior was attributed to the strain energy being released by the rotation of the dislocation cell.

We have presented experimental evidence of the progression behavior of ductile damage in an Al single crystal with prior activity of the single-slip system. This fundamental result supports the development of a nondestructive evaluation method for estimating the damage in Al, which would be used in ductile fracture investigations.

Acknowledgments

The authors would like to thank Mr. S. Tokuda of the Kitami Institute of Technology for his assistance in preparing the samples for TEM observations. The authors would like to express their sincere appreciation for the SR experiments performed at the BL28B2 beamline of SPring-8 with the approval of the Japan Synchrotron Radiation Research Institute (JASRI) Spring-8 (Proposal No. 2014B1621). This study was supported by JSPS KAKENHI (Grant No. 16K05961).

References

[1] G.Y. Deng, A.K. Tieu, L.Y. Si, L.H. Su, C. Lu, H. Wang, M. Liu, H.T. Zhu, and X.H. Liu, Influence of cold reduction on the deformation behavior and crystallographic orientation development, 81 (2014) 2-9.

[2] G. Deng, C. Lu, L. Su, A. K. Tieu, J. Liu, H. Zhu, and X. Liu, Influence of outer corner angle (OCA) on the plastic deformation and texture evolution in equal channel angular pressing, Comp. Mater. Sci., 81 (2014) 79-88.

[3] E.A. Alfyorova and D.V. Lychagin, Self-organization of plastic deformation and deformation relief in FCC single crystals, Mech. Mater., **117** (2018) 202-213.

[4] A. Godfrey, D. Juul Jensen and N. Hansen, Slip pattern microstructure and local crystallography in an aluminum single crystal of copper orientation {112}<111>, Acta Mater., **46** (1998) 835-848.

[5] M. Kobayashi and J. Shibano, Bifurcation analysis of fracture mode by simulated and experimental ductile fracture progress based on the proposed crack opening criterion, Int. J. Solids Struct., **141-142** (2018) 297-315.

[6] Y. Watanabe, T. Koike, M. Otsuka and H. Yamagata, Dynamic recrystallization of 99.999 mass% aluminum single crystals during tensile testing, J. Japan Inst. Metals, **62** (1998) 44-49.

[7] T. H. Lin, H. Q. Liu and N. G. Liamg, A micromechanical theory of fatigue crack initiation of an aluminum single crystal, Int. J. Fatigue, **25** (2003) 871-876.

[8] K. Ihara and Y. Miura, Analysis of dynamic recrystallization behavior in Al-single crystals by synchrotron radiation Laue technique, J. Japn Inst. Metals, **67** (2003) 209-217.

[9] Y. Miura, A few works on the microstructure of aluminum by means of X-ray diffraction technique, J. Japn Inst. Light Metals, **61** (2011) 544-552.

[10] C. Y. Chiem and J. Duffy, Strain rate history effects and observations of dislocation substructure in aluminum single crystals following dynamic deformation, Mater. Sci. Eng., **57** (1983) 233-247.

[11] M.J Hordon and B.L. Averbach, X-ray measurements of dislocation density in deformed copper and aluminum single crystals Acta Mater., **9** (1961) 237-246.

[12] M.J Hordon and B.L. Averbach, Precision density measurements on deformed Copper and aluminum single crystals, Acta Mater., **9** (1961) 247-249.

[13] G. K. Williamson and R. E. Smallman, III. Dislocation densities in some annealed and cold-worked metals from measurements on the X-ray debye-scherrer spectrum, Philos. Mag., **1** (1956) 34-46.

[14] J. I. Langford, A rapid method for analysing the breadths of diffraction and spectral lines using the Voigt function, J. Appl. Cryst., **11** (1978) 10-14.

[15] T. H. Keijser, E. J. Mittemeijer and H. C. F. Rozendaal, The determination of crystallite-size and lattice-strain parameters in conjunction with the profile-refinement method for the determination of crystal structures, J. Appl. Cryst., **16** (1983) 309-316.

[16] T. Ungar, S. Ott, P. G. Sanders, A. Borbely and J. R. Weertman, Dislocations, grain size and planar faults in nanostructured copper determined by high resolution X-ray diffraction and a new procedure of peak profile analysis, Acta. Mater., **46-10** (1998) 36933699.

[17] T. Ungar, Dislocation densities, arrangements and character from X-ray diffraction experiments, Mater. Sci. Eng. A, **309-310** (2001) 14-22.

[18] M. Croft et al., Strain profiling of fatigue crack overload effects using energy dispersive X-ray diffraction, Int. J. Fatigue, **27** (2005) 1408-1419.

[19] M. Rahman, M. E. Fitzpatrick, L. Edwards, M. Peel, A. Steuwer and T. Buslaps, investigation of the stress fields around a fatigue crack in aluminium alloy 5091, Mater. Sci. Forum, **571-572** (2008) 119-124.

[20] J. Shibano, M. Kiso, K. Kajiwara, T. Shobu, S. Miura and M. Kobayashi, Study on Ductile damage progress of an aluminum single crystal using synchrotron white X-ray, Mater. Sci. Forum, **768-769** (2014) 358-365.

[21] J. Shibano, K. Kajiwara, T. Tsukamoto, H. Kawai, S. Miura, S. Zhang, T. Shobu, M. Kobayashi, Evaluation of ductile damage in aluminum single crystal with prior activity of single slip system under tensile loading, Mater. Sci. Forum, **777** (2014) 176-181.

[22] R. K. Ham, The determination of dislocation densities in thin films, Philos. Mag., **6** (1961) 1183-1184.

Figure captions

Figure 1. The spots where white XRD patterns were collected along <110> and <111> under tensile loading.

Figure 2. The relative rotation angle of the normal direction of (220) in the horizontal (a) and vertical (b) planes along <111> and <110> during tensile loading from the notch.

Figure 3. The distributions of integrated intensity (a) and FWHM (b) for (220) in the vertical plane along <111> and <110> during tensile loading from the notch.

Figure 4. TEM images of the tensile loading specimen at locations (a) 0.6, (b) 0.8, (c) 1.1, and (d) 1.3 mm from the notch.

Figure 5. Enlarged TEM images of the regions (a) 0.6, (b) 0.8, (c) 1.1, and (d) 1.3 mm from the notch of the tensile loading specimen.

Figures

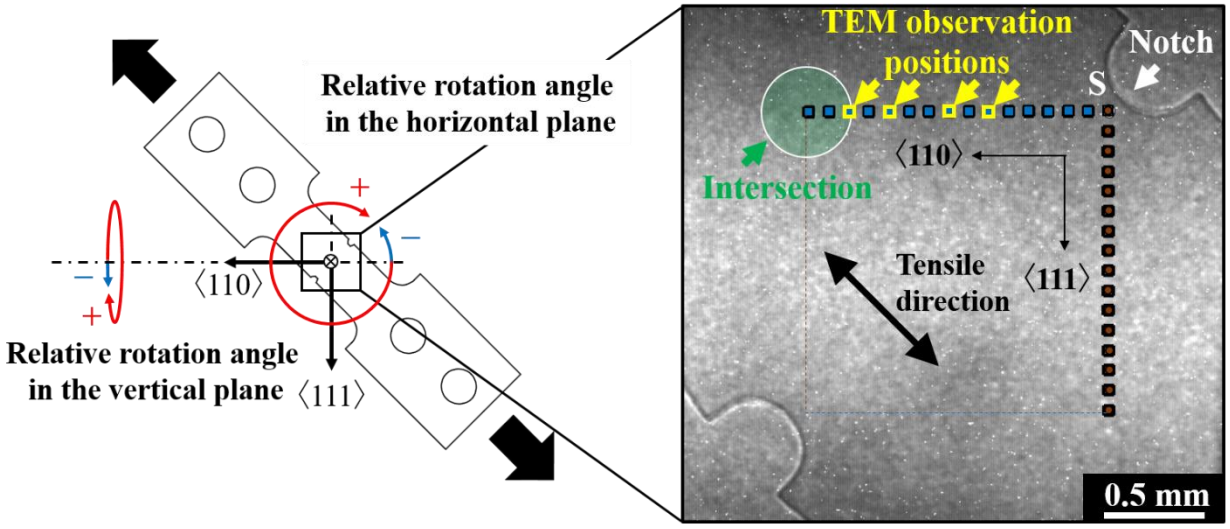

Figure 1

(a)

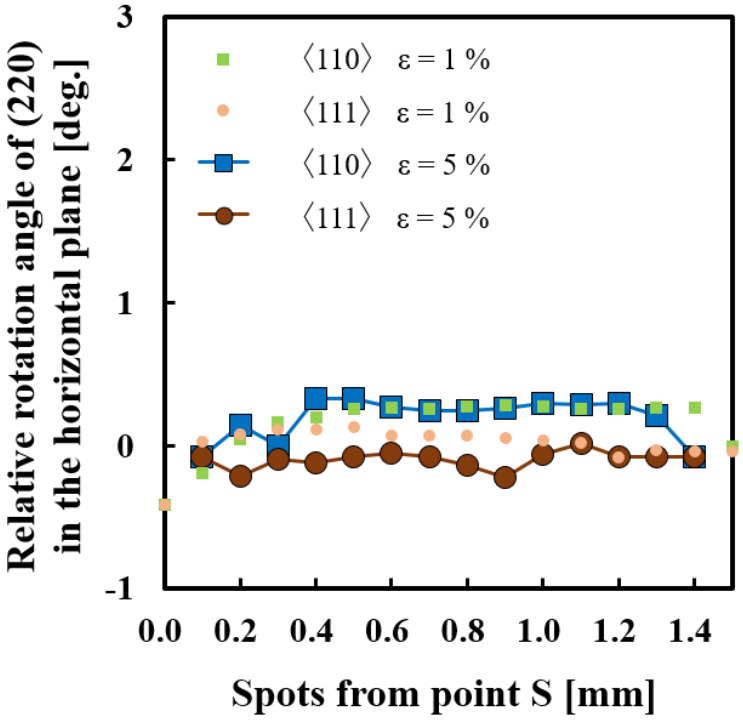
Relative rotation angle of (220) in the horizontal plane [deg.]
〈110〉 ε = 1 %
〈111〉 ε = 1 %
〈110〉 ε = 5 %
〈111〉 ε = 5 %
3
2
1
0
-1
0.0
0.2
0.4
0.6
0.8
1.0
1.2
1.4
Spots from point S [mm]

(b)

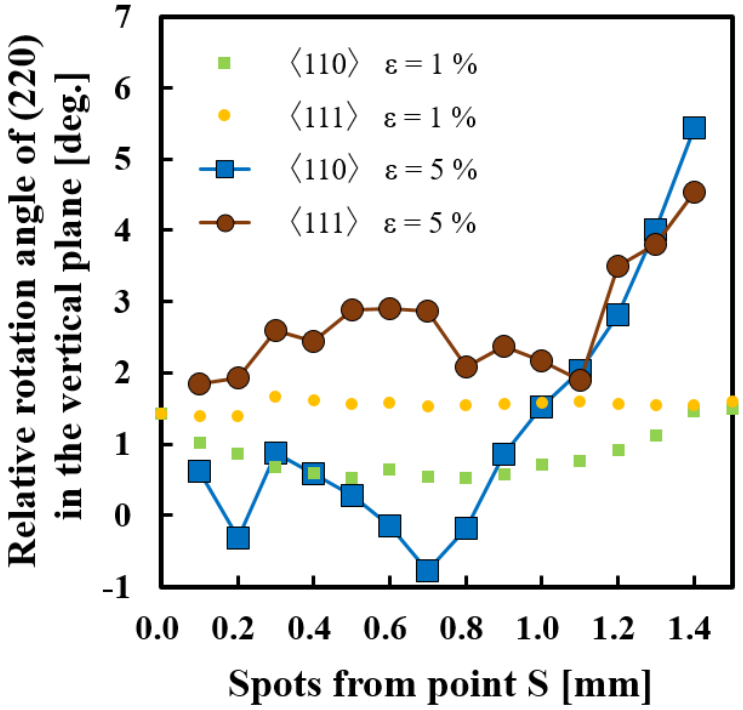
Relative rotation angle of (220) in the vertical plane [deg.]
〈110〉 ε = 1 %
〈111〉 ε = 1 %
〈110〉 ε = 5 %
〈111〉 ε = 5 %
7
6
5
4
3
2
1
0
-1
0.0
0.2
0.4
0.6
0.8
1.0
1.2
1.4
Spots from point S [mm]

Figure 2

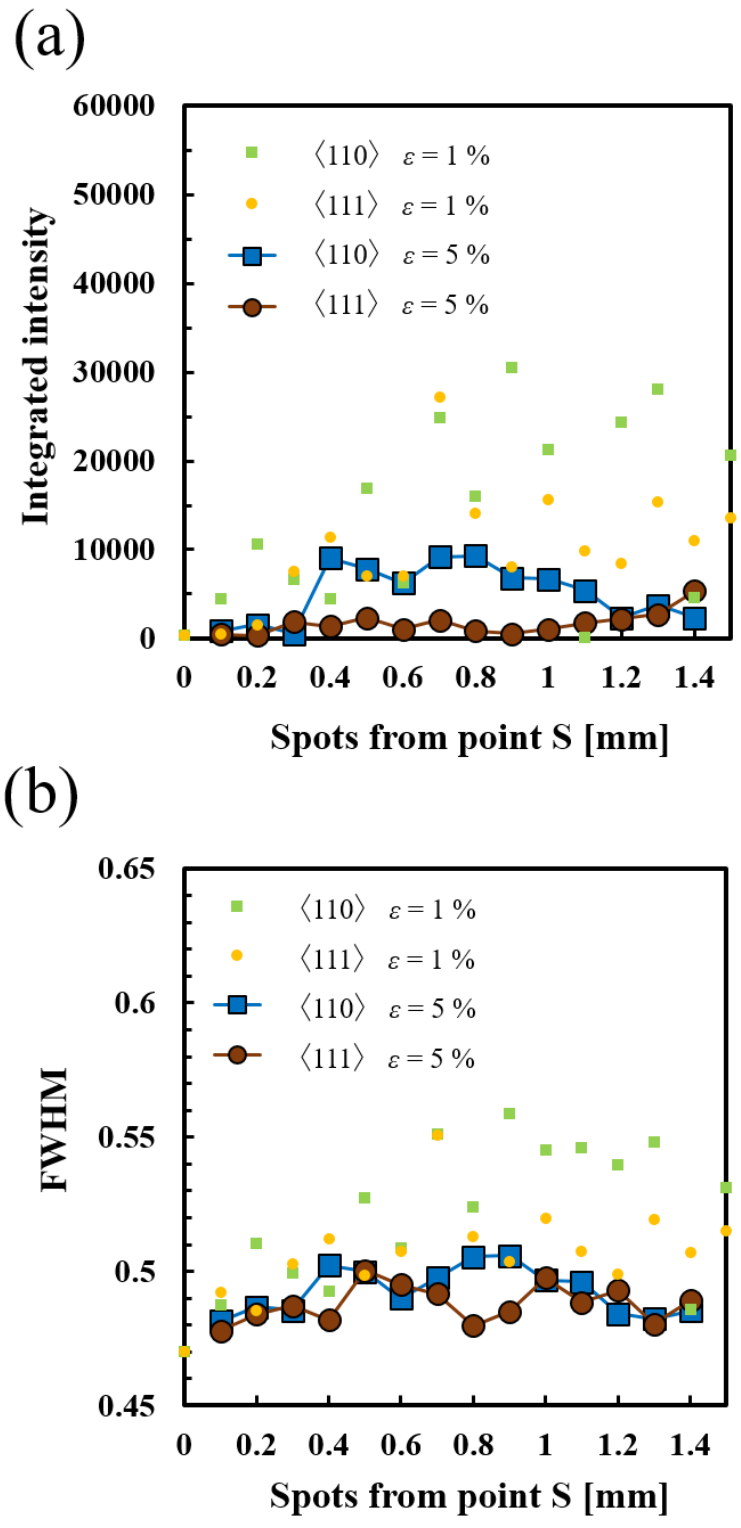

Figure 3

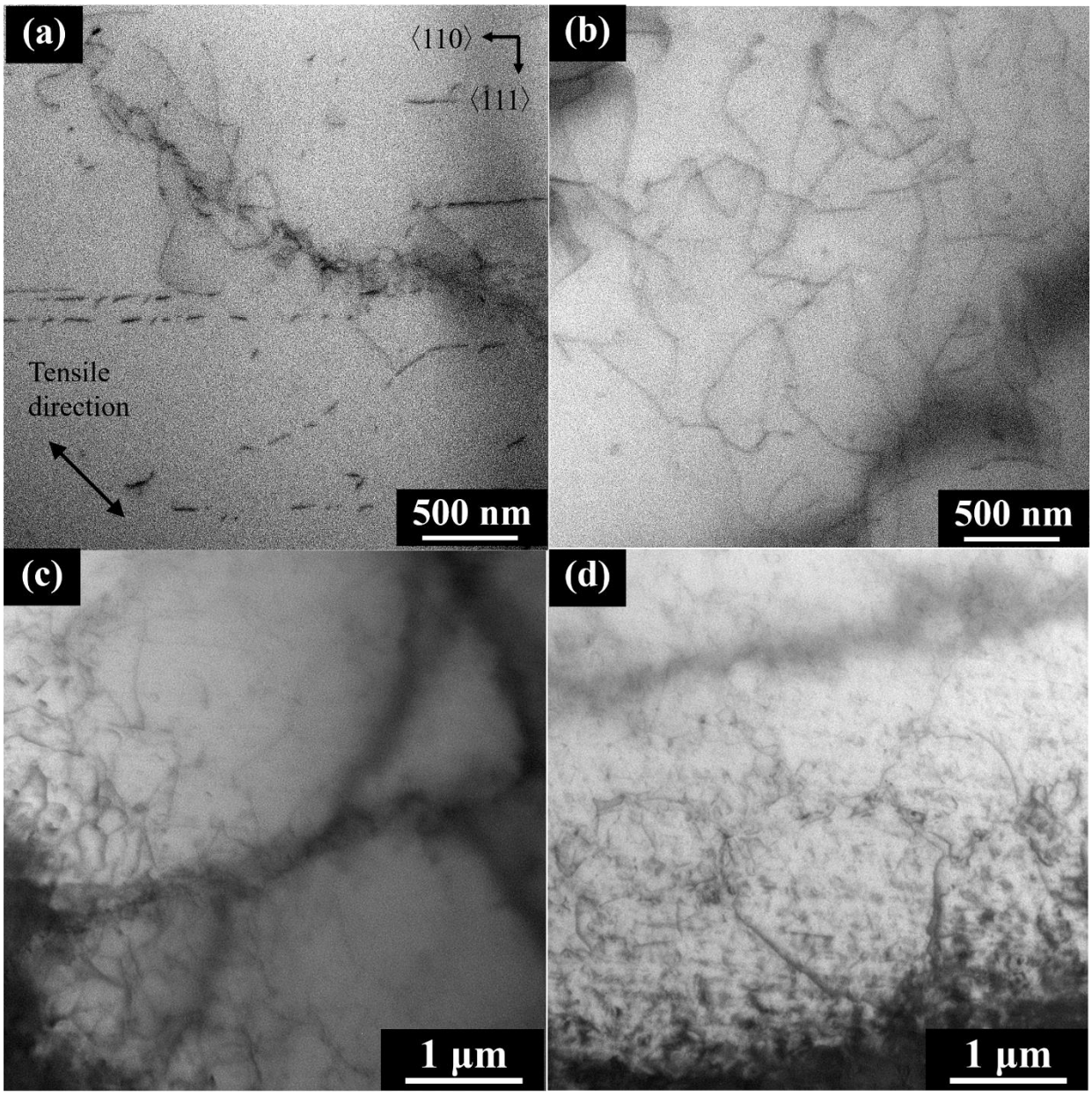

Figure 4

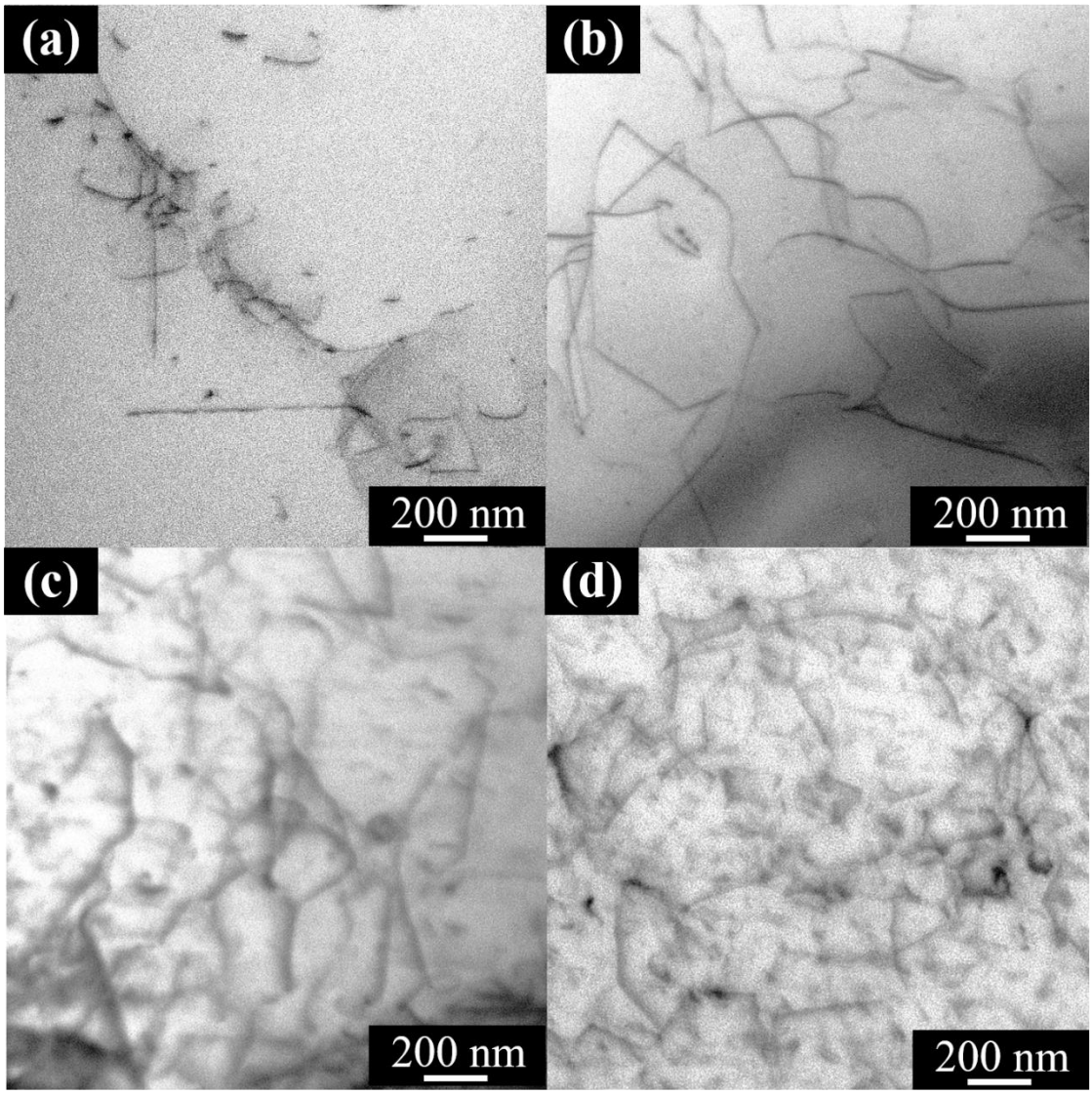

Figure 5